Wavefunction engineering in HgSe/HgTe colloidal heterostructures to enhance mid infrared photoconductive properties

Nicolas Goubet, Clément Livache, Bertille Martinez, Xiang Zhen Xu, Sandrine Ithurria, Sebastien Royer, Hervé Cruguel, Gilles Patriarche, Abdelkarim Ouerghi, Mathieu G Silly, et al.

Wavefunction engineering in HgSe/HgTe colloidal heterostructures to enhance mid infrared photoconductive properties

Nicolas Goubet[1,2], Clément Livache[1], Bertille Martinez[1], Xiang Zhen Xu[2], Sandrine Ithurria[2], Sebastien Royer[1], Hervé Cruguel[1], Gilles Patriarche[3], Abdelkarim Ouerghi[3], Mathieu Silly[5], Benoit Dubertret[2], Emmanuel Lhuillier[1*]

[1]Sorbonne Universités, UPMC Univ. Paris 06, CNRS-UMR 7588, Institut des NanoSciences de Paris, 4 place Jussieu, 75005 Paris, France
[2]Laboratoire de Physique et d'Etude des Matériaux, ESPCI-ParisTech, PSL Research University, Sorbonne Université UPMC Univ Paris 06, CNRS, 10 rue Vauquelin 75005 Paris, France.
[3] Centre de Nanosciences et de Nanotechnologies, CNRS, Univ. Paris-Sud, Université Paris-Saclay, C2N – Marcoussis, 91460 Marcoussis, France
[4]Synchrotron-SOLEIL, Saint-Aubin, BP48, F91192 Gif sur Yvette Cedex, France

Abstract : The use of intraband transition is an interesting alternative path for the design of optically active complex colloidal materials in the mid-infrared. However, so far the performance obtained for photodetection based on intraband transition remain much smaller than the one relying on interband transition in narrow band gap materials operating at the same wavelength. New strategies have to be developed to make intraband materials more effective. Here we propose to grow an heterostructure of HgSe/HgTe as a path to achieve enhanced intraband based photoconduction. We first tackle the synthetic challenge of growing an heterostructure on soft (Hg based) material. The electronic spectrum of the grown heterostructure is then investigated using a combination of numerical simulation, infrared spectroscopy, transport measurement and photoemission. We report a type II band alignment, a reduced doping compared to core only object and boosted hole conduction. Finally, we probe the photoconductive properties of the heterostructure while resonantly exciting the intraband transition by using a high power density quantum cascade laser. Compared to previous generation of material based on core only HgSe, the heterostructure have a lower dark current, stronger temperature dependence, faster photoresponse with time response below 50µs and a detectivity increased by a factor 30.

Keywords : HgSe/HgTe heterostructures, intraband transition, narrow band gap nanocrystals, mid infrared.

To whom correspondence should be sent: el@insp.upmc.fr

INTRODUCTION

Adressing the infrared range of wavelength is a material challenge where narrow band gap materials[1,2] are of utmost interest[3–7] but also present many difficulties such as a large amount of thermally activated carriers. Wavefunction engineering using wideband gap materials has been an elegant path to overcome the difficulties relatives to narrow band gap materials. In this case interband transitions are replaced by intersubband/intraband transitions. In relying on such principle, quantum well infrared photodetectors[8,9] (QWIP) and Quantum Cascade Laser[10] (QCL) have reached a great level of success as detector and source in the infrared, respectively. Up to recently, such mid infrared transitions were only possible with epitaxially grown III-V semiconductor.[11] However, a higher control of the doping level of colloidal quantum dots (CQD) have been obtained over the recent years and the growth of doped nanoparticles with mid IR transition have become a reality.[12–14] The Guyot-Sionnest's group[15] and others[16,17] even proposed recently the design of photoconductive devices where the absorption relies on intraband transition in self-doped mercury chalcogenides compounds.[18]

While the introduction of stable intraband transition in colloidal device is conceptually a breakthrough, their use into competitive device is not yet reached. Indeed, photodetectors based on intraband transition present a pretty high photoresponse,[9,19] but suffer from a large dark current, which might be inherent to intersubband/intraband device. In addition their time response is slow[15,20] (>s) and some may argue that the observed modulation purely results from bolometric effect rather than photoconduction. On the way to improve their performances, two main strategies have been explored. (*i*) To make thin film of colloidal quantum dots conductive and photoconductive, a tuning of the surface chemistry toward short molecule ensuring good inter CQD coupling is mandatory. Such increase of the conductance has indeed been observed, however it was also notice that the ligand exchange leads to a dramatic change of the absorption spectrum[21–23] due to a surface gating effect which comes as side effect of the tuning of the ligands. Such observation is both an opportunity to tune the doping level, but simultaneously leads to a dramatic sensitivity of the film to its environment. (*ii*) Alternatively, it has been proposed to synthetize core shell structures where a wide band gap material is grown over a doped core material of HgSe or HgS[24] CQD using a low temperature approach (C-ALD)[25]. Early motivation was to boost the luminescence efficiency of the intraband transition.[3,26,27] However, the introduction of the shell, similarly to the tuning of the surface chemistry, led to a complete disappearing of the intraband transition and the final material is only presenting near-IR interband transition.

The use of intraband transition remains of utmost interest, especially to push the absorption toward longer wavelengths while keeping a material with good colloidal stability, but it also requires new material approaches which will boost the performances (reduced dark current, faster time response…) while preserving the intraband absorption. In this paper, we investigate the possibility to grow HgSe/HgTe heterostructure to address this challenge. In addition to the synthetic challenge to grow a heterostructure on mechanically soft (*ie* Hg containing) material, we discuss the electronic structure of the obtained material using a combination of numerical simulation, infrared spectroscopy, electronic transport and photoemission measurements. Finally, we bring evidence for the enhanced properties of this new heterostructure compared to conventional core only HgSe CQD. In particular, films of HgSe/HgTe have lower dark current and enhanced activation energy close to half the interband gap energy. Moreover, using a quantum cascade laser as a source to resonantly excite the intraband transition, we bring an unambiguous proof for a fast (few tens of μs) photodetection based on intraband transition in a CQD based device.

DISCUSSION

The investigation of the HgSe/HgTe heterostructure starts by the exploration of its band alignment phase diagram, obtained by tuning the core and shell sizes and assuming a spherical geometry. HgSe will be used as the core material as HgSe CQDs present self-doping and intraband absorption in the mid-IR. This doping results from the narrow band-gap nature of HgSe CQDs (bulk HgSe is a semi-metal) combined with the large material work function, as discussed in ref [23]. HgTe is also a semimetal, however the presence of Te instead of Se, shifts the maximum of the valence band toward the vacuum level and make that HgTe is mostly an intrinsic (*i.e.* undoped) narrow band gap material. To further clarify the band alignment of the heterostructure, we solve the 1D time independent Schrödinger equation in spherical geometry:

$$\left[-\frac{\hbar^2}{2m^*(z)}\left(\frac{2}{r}\frac{\partial}{\partial r}+\frac{\partial^2}{\partial r^2}\right)+V(r)\right]\psi(r)=E\psi(r) \quad (1)$$

Where $\hbar$ is the reduced Planck constant, *m*(z)* the effective mass profile, *V(z)* the energy band profile, *E* the eigen energy and $\psi(r)$ the wavefunction. The numerical solving of the equation is further discussed in the supplementary informations (SI). Material input parameters are the effective mass for electron (m^*_{HgSe}=0.06m_0[28,29]; m^*_{HgTe}=0.035m_0[30,31]) and hole (m^*_{HgSe}=0.2m_0[32]; m^*_{HgTe}=0.5m_0[30,31]) and the position of the valence band maximum of the two materials. For valence band offset, we used recently proposed values (-4.7eV *vs* vacuum for HgTe and -5.5eV for HgSe) obtained from electrochemistry measurements in ref [33].

The model is rather simple since it neglects band non parabolicity, dielectric confinement[34] and assume that the core and the final heterostructures are spheres, thus we use it for qualitative discussion. Four types of band alignment have been identified, see Figure 1a. For very small core and thin shell, the confinement is strong and both electron and hole are delocalized over the whole structure, see Figure 1b. In this case only interband transitions are expected. As the size of the shell is increased, see Figure 1c, the hole gets localized in the HgTe shell, while the electron stays delocalized, corresponding to a quasi-type II band alignment. Inversely if the size of the core is increased, see Figure 1d, the electron gets less confined and localizes in the HgSe core. The energy of the 1S electronic state drops below the Fermi level of the system (at -4.7 eV below vacuum according to ref [17]) and intraband transition appears, while the interband transition also presents a quasi-type II band alignment, yet inverted compared to the zone 2. For large core and shell, see Figure 1e, electron and hole are localized respectively in the core and in the shell, thus the interband transition acquires a real type II character. Moreover, intraband electronic transition is also expected in this range of sizes. This area of the phase diagram is of great interest since it combines intraband transition and a poor overlap of the electron hole pair which will prevent detrimental recombination for photo-excited electron.

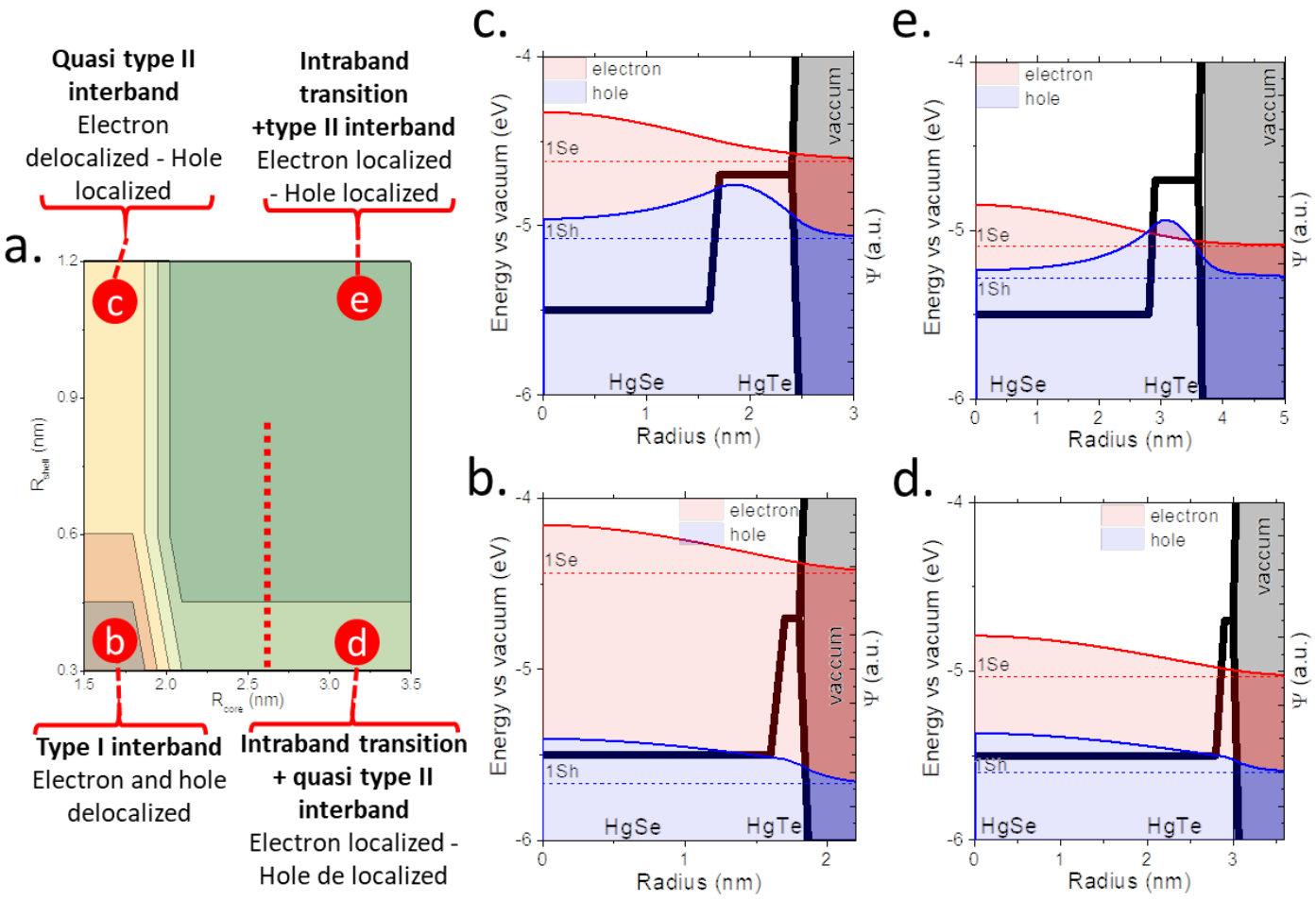

Figure 1 a. Phase diagram for the band alignment of an HgSe/HgTe heterostructure as a function of the core diameter and the HgTe shell thickness. The red dashed line corresponds to the grown heterostructure later in the text. b, c, d and e describe the energy profiles and wavefunctions for area of the phase diagram labeled with the same letter. The energy profile of the bulk valence and conduction band appears as bold black line. Due to the semimetal nature of HgSe and HgTe valence band and conduction band touch each other. Blue and red lines are respectively the hole and electeron wavefunction. These curves have been shifted from zero, in order that the null density of presence of the wavefunction corresponds to the eigen energy associated with each state.

To chemically grow a heterostructure made of HgSe/HgTe presenting an intraband transition, we first synthetize cores of HgSe, with typical size around 5.2 ± 0.7 nm according to the procedure given in ref [17], see electron microscopy of the obtained material in Figure 2a. The material has a zinc blende structure according to its X-ray diffraction pattern (Figure 2c). Its optical spectrum is made of an intraband transition around 2500 cm^{-1} (≈300 meV) and a broad interband signal above 7000 cm^{-1} (840 meV), see Figure 3a. Being soft materials, mercury chalcogenides are grown at low temperature, they tends to quickly sinter into µm scale objects once exposed to high temperature[35]. As a result most of the efforts dedicated to grow a heterostructure of Hg based material are based on the low temperature colloidal ALD (C-ALD) procedure. This procedure is easy to implement for sulfide and selenide but far more complicated in the case of telluride material due to the fast oxidation of Te. Here, we propose an alternative method where mercury precursor (HgI_2) is mixed with HgSe cores and Te precursor (TOPTe) is introduced dropwise at a mild temperature (60-100°C) with optimum temperature at 80°C. Note that the choice of HgI_2 precursor is motivated by its lower reactivity compared to other halide, when forming HgTe.[36] The reaction with other halides or mercury oleate is also possible but leads to a lower control of the final shape of the heterostructure and to stronger secondary nucleation. Indeed, due

to their high reactivity with TOPTe, reaction with $HgBr_2$ and $HgCl_2$ leads to large nanocrystals (10-15nm) attributed to side nucleation, see Figure S2 and S3.

As shown in transmission electron microscopy (TEM) images in Figure 2c-d and Figure S1, we obtain heterostructures with a final mean diameter around 6.4± 1.3 nm, corresponding to the growth of one lattice parameter of HgTe all around the HgSe core. Note that the final material still presents a small size and is colloidally stable which is key feature for the future integration of the material into geometry devices. TEM reveals that the shape deviate from a sphere, see inset of Figure 2b-d, where in addition of core shell structure we observe januslike nanoparticles where some Se rich part are epitaxially connected to Te rich part, see Figure 2d-f. While this shape deviation can introduce quantitative deviation compared to simulation, the main results: (*i*) presence of intraband transition in the HgSe part and (ii) type II band alignment between the two materials remain unaffected. The X-ray diffraction combined with energy dispersive X-ray spectroscopy (EDX) conducted with different amount of growth material confirms the presence of both HgSe and HgTe phases, see Figure 2g and S1b.

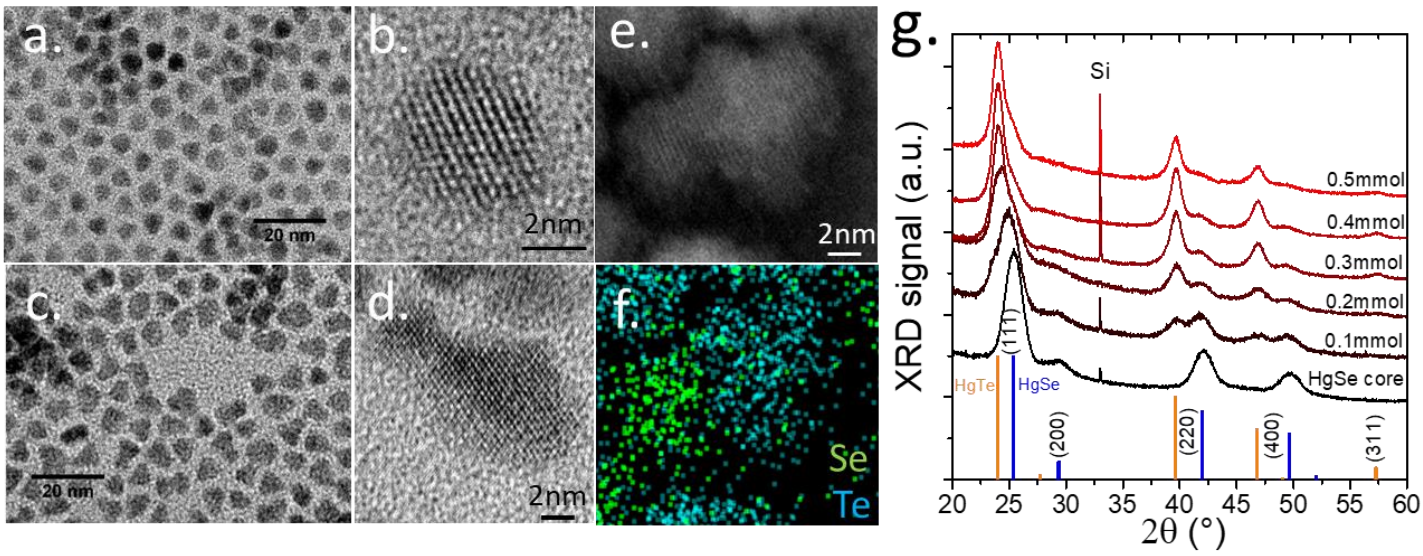

Figure 2 a. and b. Low and high-resolution TEM images of the HgSe core, respectively. c. and d. Low and high-resolution TEM images of the HgSe/HgTe heterostructure nanocrystals. e. HAADF STEM image of an HgSe/HgTe heterostructure and (f) the localization of the Se and Te from EDX mapping. g. X-Ray diffraction patterns for the HgSe core and for the HgSe/HgTe heterostructure with different amounts of HgTe. Orange and blue diffraction peaks for the bulk HgTe and HgSe, respectively.

As the amount of HgTe is increased, we observe a clear modification of the optical spectrum, see Figure 3a. Overall the intraband signal stays unchanged, with only a slight broadening toward the low wavenumber part of the spectrum. It is the first colloidal heterostructure which preserves the intraband signal in presence of an epitaxially grown shell. On the other hand, the part relative to interband transition is far more affected. At first, we observe a debleaching of the $1S_h$-$1S_e$ transition as evidenced by the appearing of an excitonic feature at 5500 cm^{-1}. This suggests a filling of the heterostructure close to 2 electrons per CQD, as confirmed by optical[23] and photoemission measurements[21]. Then, as more HgTe is introduced, this new feature is redshifted and finally saturates around 4000 cm^{-1}. The final energy of this peak depends on the growth temperature. The higher the temperature of the shell growth, the reddest the feature, see figure S3. Typically the interband transitions falls around 5000 cm^{-1} while the reaction temperature is 60 °C and is pushed to 3500 cm^{-1} for a reaction at 100 °C. In this case, interband and intraband signal spectrally overlap and make their interpretation more complex.

As HgSe and HgTe are epitaxially connected, we may believe that the observed change of the optical spectrum may result from the strain induced by the shell on the core. XRD indeed reveals a 4% change in the HgSe lattice parameter as the shell is grown, see figure S4. It is thus of utmost interest to quantify how the induced pressure will affect the spectrum. The lattice parameter of the shell (a_{HgTe}=0.6453 nm) is larger than the one of the core (a_{HgSe}=0.6085 nm). The epitaxial growth implies that HgSe will tend to expand while the shell is constrained. In our case the mismatch is $\varepsilon = \frac{a_{core} - a_{shell}}{a_{core}} \approx -0.06$. Assuming a spherical symmetry for the core shell heterostructure, the pressure at the core shell interface is given by

$$P_0 = \frac{2E_{core}E_{shell}\varepsilon\left(\frac{R_{shell}^{\ 3}}{R_{core}^{\ 3}} - 1\right)}{\left(2E_{shell}(1-2\upsilon_{core}) + E_{core}(1+\upsilon_{shell})\right)\frac{R_{shell}^{\ 3}}{R_{core}^{\ 3}} - 2\left(E_{shell}(1-2\upsilon_{core}) - E_{core}(1-2\upsilon_{shell})\right)}$$

Where *E* is the young modulus and υ the Poisson ratio. Given the vicinity of HgSe and HgTe materials and given the large spreading of the reported values for their mechanical parameters, It is reasonable to assume $E_{core}=E_{shell}=E$=40 GPa[37] and $\nu_{core}=\nu_{shell}=\nu$=0.46.[38] This allows simplifying the expression of the pressure to

$$P_0 = \frac{2E\varepsilon\left(\frac{R_{shell}^{\ 3}}{R_{core}^{\ 3}} - 1\right)}{3(1-\upsilon)\frac{R_{shell}^{\ 3}}{R_{core}^{\ 3}}} \approx 1.4GPa$$

The evaluation of the band edge shift expected to result from the induced pressure is given by $\delta E = a_p P_0$, with a_p*=4.9 meV/kbar*[39] the deformation potential due to pressure. We end up with a value of the shift due to pressure of only 68 meV, which is smaller than the measured shift of the interband transition (1500 cm^{-1} or 180 meV). As a result, pressure is not enough to explain the experimental shift which can be mostly attributed to a change of band profile.

We then further refine our simulation model to include the electrostatic effects due to the presence of electron and to excess of cation localized on the surface of the CQD.[40] It was indeed recently suggested by Liu *et al*[41], in a very inspiring paper that non stoichiometry may induce some severe modifications of the energy band profile. Thus we self-consistently solve the Poisson and Schrodinger equation, see SI for details. The presence of Hg excess cation results in a bending of the bands away from the vacuum level close to the surface of the nanocrystal, see figure S9, which further favor the injection of electrons within the CQD quantum states. Our simulation reveals that the electron wavefunction stays confined in HgSe and is overall poorly affected by the growth of the shell whereas the hole wavefunction is strongly impacted, see Figure 3c. The energy of the 1Se state is poorly affected by the presence of the shell, which is consistent with the absence of shift of the intraband signal. Due to the band offset between HgSe and HgTe, the hole tends to be located into HgTe, see Figure 3d, which result in a severe shift of the energy of the 1Sh state. However, due to significant deviation from an ideal spherical core-shell geometry, no quantitative agreement should be expected.

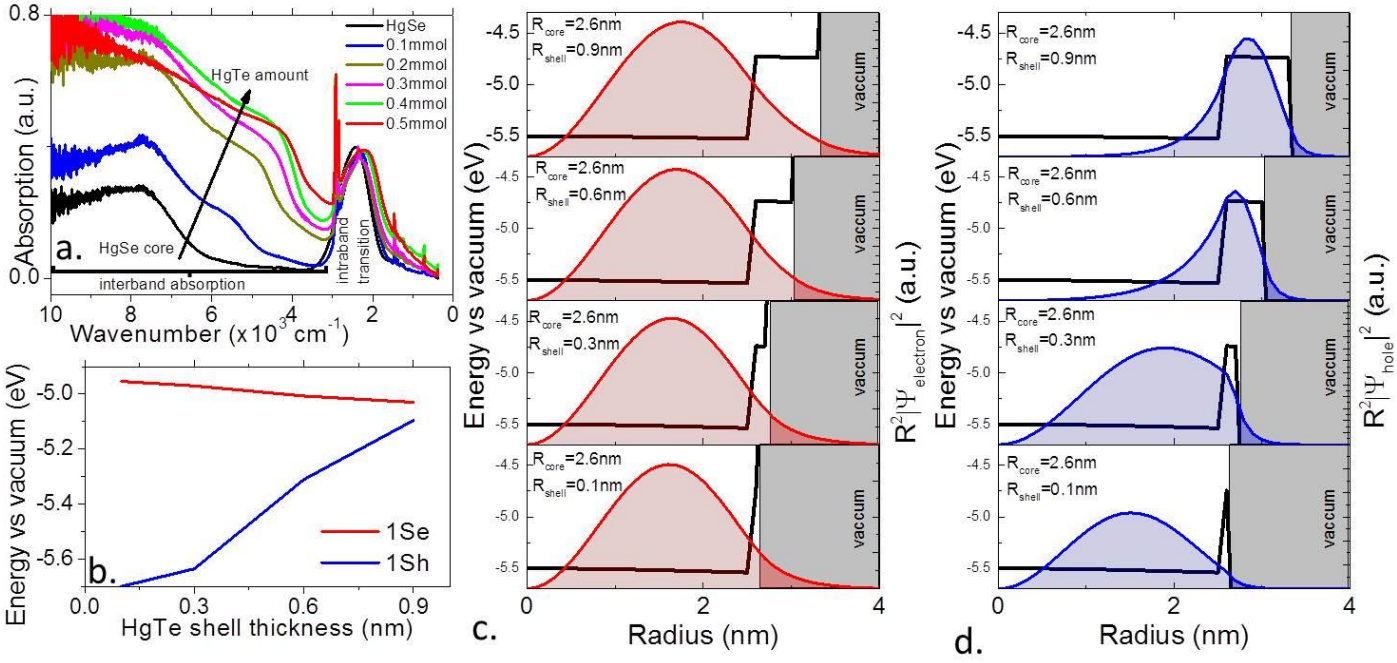

Figure 3 a. absorption spectra of HgSe core and HgSe/HgTe core shell structure for different amount of HgTe. The intraband signal is barely affected by the addition of HgTe, while the interband signal is amplified and redshifted. b. Energy of the 1Se and 1Sh state of an HgSe/HgTe heterostructure (2.6 nm of radius size for the HgSe core) as a function of the HgTe thickness. c. Conduction band profile and electron density distribution for different values of the shell thickness. d. Valence band profile and hole density distribution for different values of the shell thickness.

Further modifications of the electronic properties resulting from the heterostructure formation can be revealed using electronic transport combined with photoemission measurements. Transport is probed using an ion-gel electrolyte configuration, see methods and reference [42] for more details on the sample preparation and Supplementary Information for a scheme of the device. HgSe is a n-type material, see Figure 4a, with non-monotonic transfer curve due to Pauli blockade when the 1Se state gets fully filled (*ie* at 2 electrons per CQD).[17] As HgTe is grown on HgSe core, the material turns ambipolar and both hole and electron conduction are noticeable, see Figure 4b and S9. As expected, the HgSe/HgTe heterostructure present an intermediate behavior in term of hole mobility between HgSe (without hole conduction) and HgTe for which electron and hole mobilities are quite close, see Figure 4c. This change of behavior can be understood thanks to photoemission. Initially in HgSe, the energy from Fermi level to valence band (V_b-E_F)is 1.07eV, which corresponds to the sum of the interband energy and intraband transition in the HgSe core and means that Fermi level is almost resonant with the 1Pe state, see Figure 4e. This observation is consistent with full bleaching of the interband optical transition. A zoom on the low binding energy part (*ie* close to the Fermi level) of the spectrum reveals that the quantity V_b-E_F is decreasing while the HgTe amount is increased, see the inset of Figure 4d as well as Figure S7 and S8. Finally, the Fermi level end up being resonant with the 1Se state, corresponding to roughly ≈1 electron per CQD and is further confirmed by the fact that intraband and interband absorption present similar magnitudes. Thanks to this measurement we can propose an effective absolute energy spectrum for the heterostructure, see Figure 4e.

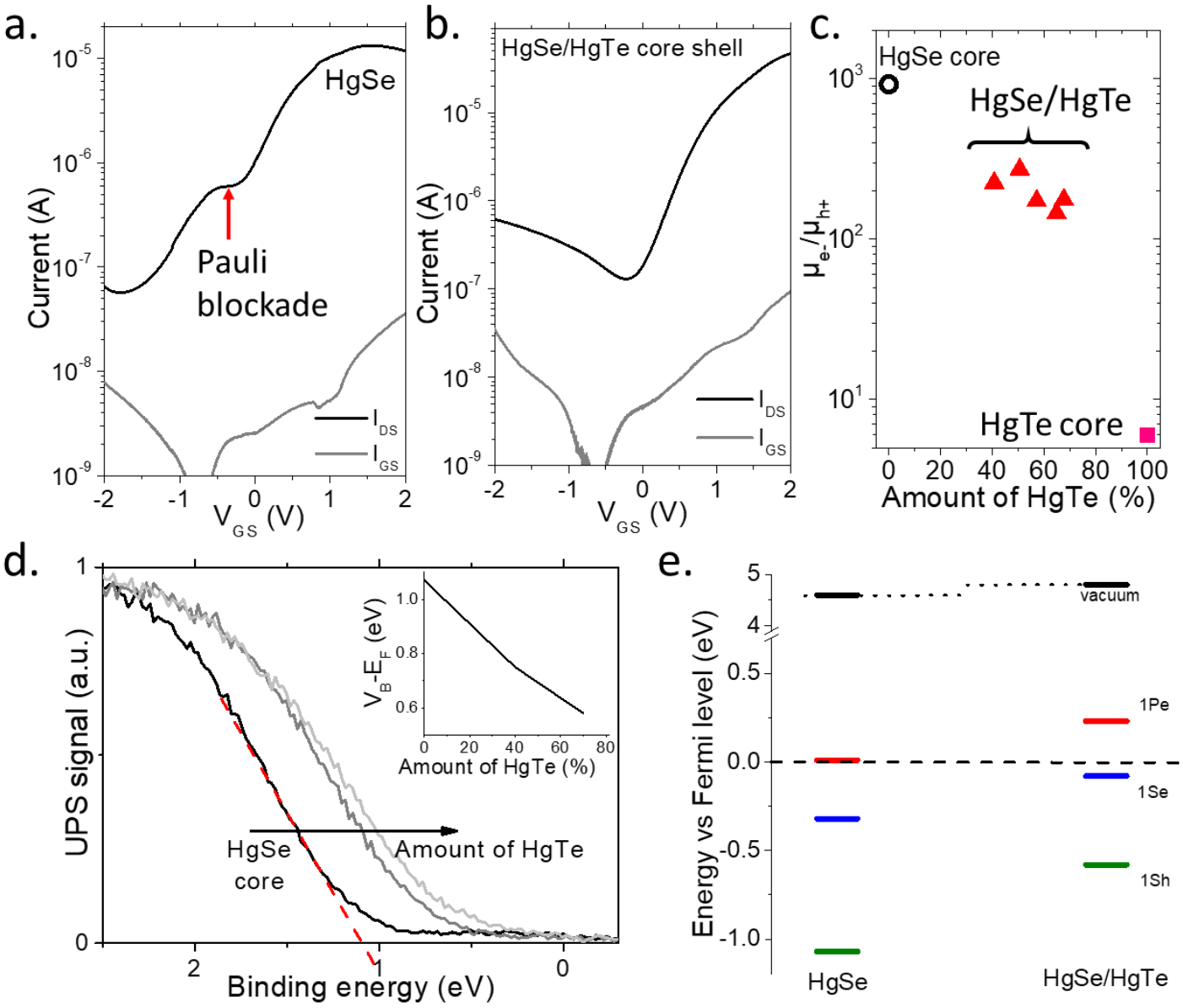

Figure 4 a. Transfer curve (drain current as a function of gate bias) for a thin film of HgSe CQD used as channel of an electrolyte gated transistor. b. Transfer curve for a thin film of HgSe/HgTe CQD used as channel of an electrolyte-gated transistor. c Ratio of the electronic mobility over the hole mobility for HgSe/HgTe heterostructure with different amount of the two materials. d. Photoemission signal relative to the valence band for a film of HgSe/HgTe CQD with different ratio of HgTe. The inset gives the relative energy of the valence band with respect to the Fermi level as a function of the amount of HgTe. e. Reconstructed effective electronic spectrum for HgSe core and HgSe/HgTe heterostructure in absolute energy scale.

It is critical to determine and quantify how the heterostructure behave once used as active layer of a mid IR photodetector. A first noticeable difference is that for similar film thickness (≈100 nm), the resistance of the heterostructure is much higher (≈100 kΩ) than the one reported for core only object (≈10 kΩ). This reduction of the dark current mainly results from the reduction of doping. The temperature dependence of the current reveals another key improvement, see Figure 5a. HgSe presents a poor temperature dependence and the activation energy of the current around room temperature present a low activation of only 40 meV. In other words, not only HgSe is presenting a large dark current, but cooling even barely improves the performance level. HgSe/HgTe heterostructures present a strongly enhanced temperature dependence. The current drops by five orders of magnitude between 300 K and 20 K, see Figure 5a. The activation energy of the material around room temperature is now estimated to be 180 meV, which

is just below the intraband energy and quite close to half the interband energy. One can also note that the obtained value is very similar to the one obtained for pure HgTe CQD, see figure S12.

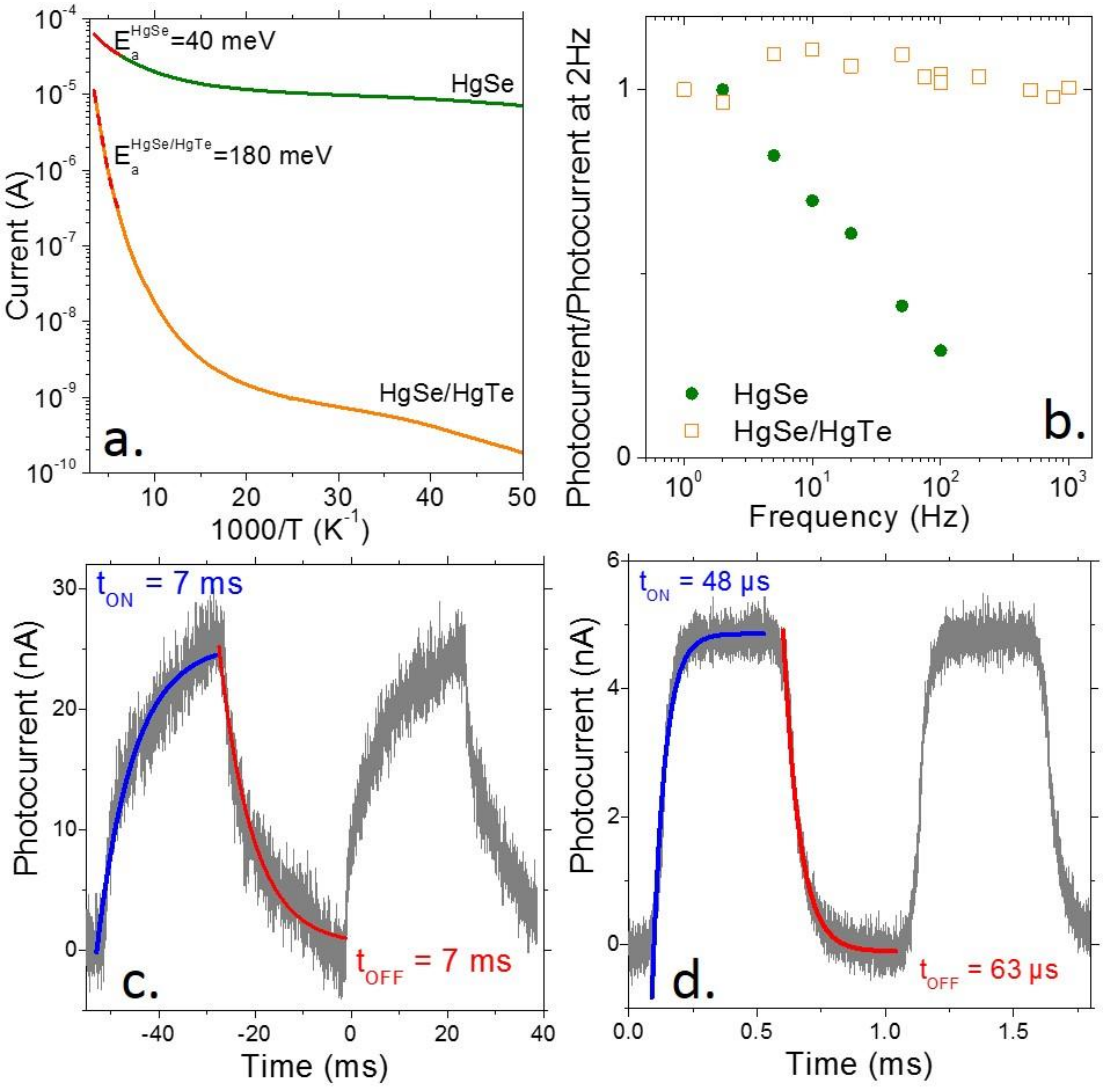

Figure 5 a. Current as a function of the temperature for thin film made of HgSe core and for an HgSe/HgTe heterostructure. The Arrhenius fit close to room temperature range is highlighted in red. b. Bode diagram (normalized signal magnitude) as a function of the signal frequency for thin film made of HgSe core and for an HgSe/HgTe heterostructure. c Temporal evolution of the photoresponse from an HgSe CQD film while the light (4.4 µm QCL- 8 mW of incident power) is modulated at 10 Hz. d. Temporal evolution of the photoresponse from an HgSe/HgTe heterostructure film while the light (4.4 µm QCL- 8 mW of incident power) is modulated at 1 kHz.

The time response of the devices made with core only material or heterostructures is also investigated: we probe the selectively the intraband photoresponse by exciting the system with a high power density quantum cascade laser operating at 4.4 µm (2200-2300 cm^{-1}). Again, HgSe films present a slow time response, as revealed in the frequency domain by the rapidly decaying Bode diagram or in the time domain with a rise/decay time of 7 ms. The HgSe/HgTe heterostructure presents a much faster photoresponse with a flat Bode diagram up to 1 kHz. The corresponding time response is estimated to be around 50 µs and is actually limited by the speed of the mechanical chopper used for the measurements. Such fast photoresponse is unlikely to result from a bolometric effect and thus can be fully attributed to photoconduction. To our understanding, the fastening of the photoresponse is the result of two effects. For a given surface chemistry, HgTe present a higher mobility than HgSe,[33] contributing for a small factor 10 to 100 in the fastening of the time reponse: under interband excitation, HgTe presents a much faster time response than HgSe because of the better charge carrier mobility. Since HgSe in only a n-type material, under interband excitation, the hole stay trapped. To preserve the material neutrality, electrons will flow and recirculate as long as the hole remains (*ie* until it gets

recombined with an electron or with some environment molecule). This generates gain[43] but slows down the response since the latter is now driven by the minority carrier trapping time. In HgSe/HgTe heterostructure, as predicted in our simulation, see Figure 1 ans S5, there is an interband absorption which is now overlapping with the intraband transition. The latter has a type II character with the hole localized in HgTe and the electron in HgSe. In this transition the electron and hole are inherently spatially separated which unfavors their recombination and trapping, while giving them a interband character similar to that of HgTe, hence allowing for fast detection

To finish, we have measured the responsivity and noise current density of a thin film made of pure HgSe and from HgSe/HgTe heterostructure, see figure S13 and S14 to determine their relative specific detectivity (*ie* signal to noise ratio). As expected for nanocrystal film the noise is limited by its 1/f contribution,[44] see figure S14. We have determined that at room temperature and low frequency (10 Hz) the detectivity of the heterostructured material is already 30 times higher than the value obtained for pure HgSe, while these conditions do not benefit from all improvements (larger activation energy and faster response) obtained in HgSe/HgTe.

CONCLUSION

So far, devices relying on intraband transitions into colloidal CQD were suffering from key limitations preventing the obtention of competitive performances. Moreover, most attempts to tune the material were leading to a partial or complete disappearing of the intraband signal. Here we demonstrate the growth of HgSe/HgTe heterostruture, where the intraband signal is preserved. We investigate the electronic spectrum of this material using a combination of numerical simulation, infrared spectroscopy, electronic transport and photoemission measurements. We bring evidence for a type II band alignment in our heterostructure, a reduced doping compared to pure HgSe core and enhanced hole mobility. This modified spectrum is then used to obtain enhanced mid IR photonductive performances, with a reduced dark current, stronger temperature dependence (*ie* even more dark current reduction at low temperature), accelerated photoresponse with time response faster than 50 µs and increased detectivity by a factor 30. Our strategy is very promising to bring performances of intraband-based materials to the same level of interband-based materials.

ACKNOWLEDEGMENTS

EL thanks the support ERC starting grant blackQD. We acknowledge the use of clean-room facilities from the "Centrale de Proximité Paris-Centre". This work has been supported by the Region Ile-de-France in the framework of DIM Nano-K (grant dopQD). This work was supported by French state funds managed by the ANR within the Investissements d'Avenir programme under reference ANR-11-IDEX-0004-02, and more specifically within the framework of the Cluster of Excellence MATISSE and also by the grant Nanodose and H2DH. NG thank Nexdot for post doc funding.

REFERENCES

(1) Keuleyan, S.; Lhuillier, E.; Brajuskovic, V.; Guyot-Sionnest, P. Mid-Infrared HgTe Colloidal Quantum Dot Photodetectors. *Nat. Photonics* **2011**, *5* (8), 489–493.

(2) Kovalenko, M. V.; Kaufmann, E.; Pachinger, D.; Roither, J.; Huber, M.; Stangl, J.; Hesser, G.; Schäffler, F.; Heiss, W. Colloidal HgTe Nanocrystals with Widely Tunable Narrow Band Gap Energies: From Telecommunications to Molecular Vibrations. *J. Am. Chem. Soc.* **2006**, *128* (11), 3516–3517.

(3) Geiregat, P.; Houtepen, A. J.; Sagar, L. K.; Infante, I.; Zapata, F.; Grigel, V.; Allan, G.; Delerue, C.; Thourhout, D. V.; Hens, Z. Continuous-Wave Infrared Optical Gain and Amplified Spontaneous Emission at Ultralow Threshold by Colloidal HgTe Quantum Dots. *Nat. Mater.* **2017**.

(4) Chen, M.; Lu, H.; Abdelazim, N. M.; Zhu, Y.; Wang, Z.; Ren, W.; Kershaw, S. V.; Rogach, A. L.; Zhao, N. Mercury Telluride Quantum Dot Based Phototransistor Enabling High-Sensitivity Room-Temperature Photodetection at 2000 Nm. *ACS Nano* **2017**, *11* (6), 5614–5622.
(5) Tang, X.; Wu, G. fu; Lai, K. W. C. Plasmon Resonance Enhanced Colloidal HgSe Quantum Dot Filterless Narrowband Photodetectors for Mid-Wave Infrared. *J. Mater. Chem. C* **2017**, *5* (2), 362–369.
(6) Tang, X.; Tang, X.; Lai, K. W. C. Scalable Fabrication of Infrared Detectors with Multispectral Photoresponse Based on Patterned Colloidal Quantum Dot Films. *ACS Photonics* **2016**, *3* (12), 2396–2404.
(7) Kershaw, S. V.; Susha, A. S.; Rogach, A. L. Narrow Bandgap Colloidal Metal Chalcogenide Quantum Dots: Synthetic Methods, Heterostructures, Assemblies, Electronic and Infrared Optical Properties. *Chem. Soc. Rev.* **2013**, *42* (7), 3033–3087.
(8) Levine, B. F. Quantum-well Infrared Photodetectors. *J. Appl. Phys.* **1993**, *74* (8), R1–R81.
(9) Schneider, H.; Liu, H. *Quantum Well Infrared Photodetectors - Physics and | Harald Schneider | Springer*; 2007.
(10) Faist, J.; Capasso, F.; Sivco, D. L.; Sirtori, C.; Hutchinson, A. L.; Cho, A. Y. Quantum Cascade Laser. *Science* **1994**, *264* (5158), 553–556.
(11) Rogalski, A.; Antoszewski, J.; Faraone, L. Third-Generation Infrared Photodetector Arrays. *J. Appl. Phys.* **2009**, *105* (9), 091101.
(12) Schimpf, A. M.; Lounis, S. D.; Runnerstrom, E. L.; Milliron, D. J.; Gamelin, D. R. Redox Chemistries and Plasmon Energies of Photodoped In2O3 and Sn-Doped In2O3 (ITO) Nanocrystals. *J. Am. Chem. Soc.* **2015**, *137* (1), 518–524.
(13) Jeong, K. S.; Deng, Z.; Keuleyan, S.; Liu, H.; Guyot-Sionnest, P. Air-Stable N-Doped Colloidal HgS Quantum Dots. *J. Phys. Chem. Lett.* **2014**, *5* (7), 1139–1143.
(14) Gresback, R.; Kramer, N. J.; Ding, Y.; Chen, T.; Kortshagen, U. R.; Nozaki, T. Controlled Doping of Silicon Nanocrystals Investigated by Solution-Processed Field Effect Transistors. *ACS Nano* **2014**, *8* (6), 5650–5656.
(15) Deng, Z.; Jeong, K. S.; Guyot-Sionnest, P. Colloidal Quantum Dots Intraband Photodetectors. *ACS Nano* **2014**, *8* (11), 11707–11714.
(16) Jeong, J.; Yoon, B.; Kwon, Y.-W.; Choi, D.; Jeong, K. S. Singly and Doubly Occupied Higher Quantum States in Nanocrystals. *Nano Lett.* **2017**, *17* (2), 1187–1193.
(17) Lhuillier, E.; Scarafagio, M.; Hease, P.; Nadal, B.; Aubin, H.; Xu, X. Z.; Lequeux, N.; Patriarche, G.; Ithurria, S.; Dubertret, B. Infrared Photodetection Based on Colloidal Quantum-Dot Films with High Mobility and Optical Absorption up to THz. *Nano Lett.* **2016**, *16* (2), 1282–1286.
(18) Lhuillier, E.; Guyot-Sionnest, P. Recent Progresses in Mid Infrared Nanocrystal Optoelectronics. *IEEE J. Sel. Top. Quantum Electron.* **2017**, *23* (5), 1–8.
(19) Wang, H.; Lhuillier, E.; Yu, Q.; Zimmers, A.; Dubertret, B.; Ulysse, C.; Aubin, H. Transport in a Single Self-Doped Nanocrystal. *ACS Nano* **2017**, *11* (2), 1222–1229.
(20) Choi, D.; Yoon, B.; Kim, D.-K.; Baik, H.; Choi, J.-H.; Jeong, K. S. Major Electronic Transition Shift from Bandgap to Localized Surface Plasmon Resonance in CdxHg1–xSe Alloy Nanocrystals. *Chem. Mater.* **2017**, *29* (19), 8548–8554.
(21) Brown, P. R.; Kim, D.; Lunt, R. R.; Zhao, N.; Bawendi, M. G.; Grossman, J. C.; Bulović, V. Energy Level Modification in Lead Sulfide Quantum Dot Thin Films through Ligand Exchange. *ACS Nano* **2014**, *8* (6), 5863–5872.
(22) Martinez, B.; Livache, C.; Notemgnou Mouafo, L. D.; Goubet, N.; Keuleyan, S.; Cruguel, H.; Ithurria, S.; Aubin, H.; Ouerghi, A.; Doudin, B.; et al. HgSe Self-Doped Nanocrystals as a Platform to Investigate the Effects of Vanishing Confinement. *ACS Appl. Mater. Interfaces* **2017**, *9* (41), 36173–36180.
(23) Robin, A.; Livache, C.; Ithurria, S.; Lacaze, E.; Dubertret, B.; Lhuillier, E. Surface Control of Doping in Self-Doped Nanocrystals. *ACS Appl. Mater. Interfaces* **2016**, *8* (40), 27122–27128.
(24) Shen, G.; Guyot-Sionnest, P. HgS and HgS/CdS Colloidal Quantum Dots with Infrared Intraband Transitions and Emergence of a Surface Plasmon. *J. Phys. Chem. C* **2016**, *120* (21), 11744–11753.
(25) Ithurria, S.; Talapin, D. V. Colloidal Atomic Layer Deposition (c-ALD) Using Self-Limiting Reactions at Nanocrystal Surface Coupled to Phase Transfer between Polar and Nonpolar Media. *J. Am. Chem. Soc.* **2012**, *134* (45), 18585–18590.
(26) Sagar, L. K.; Walravens, W.; Maes, J.; Geiregat, P.; Hens, Z. HgSe/CdE (E = S, Se) Core/Shell Nanocrystals by Colloidal Atomic Layer Deposition. *J. Phys. Chem. C* **2017**, *121* (25), 13816–13822.
(27) Deng, Z.; Guyot-Sionnest, P. Intraband Luminescence from HgSe/CdS Core/Shell Quantum Dots. *ACS Nano* **2016**, *10* (2), 2121–2127.

(28) Wright, G. B.; Strauss, A. J.; Harman, T. C. Nonparabolic Conduction Band in HgSe and HgSe(0.5)Te(0.5). *Phys. Rev.* **1962**, *125* (5), 1534–1536.
(29) Seiler, D. G.; Galazka, R. R.; Becker, W. M. Band Structure of HgSe: Band Parameter Determinations from Effective-Mass Data, and Concentration Dependence and Anisotropy of Beating Effects in the Shubnikov-de Haas Oscillations. *Phys. Rev. B* **1971**, *3* (12), 4274–4285.
(30) Dornhaus, R.; Nimtz, G. *Narrow-Gap Semiconductors*; Springer, 2006.
(31) Śniadower, L.; Ivanov-Omsky, V. I.; Dziuba, Z. Determination of the Effective Mass of Electrons in HgTe. *Phys. Status Solidi B* **1965**, *8* (1), K43–K45.
(32) Harman, T. C.; Strauss, A. J. Band Structure of HgSe and HgSe–HgTe Alloys. *J. Appl. Phys.* **1961**, *32* (10), 2265–2270.
(33) Chen, M.; Guyot-Sionnest, P. Reversible Electrochemistry of Mercury Chalcogenide Colloidal Quantum Dot Films. *ACS Nano* **2017**, *11* (4), 4165–4173.
(34) Rodina, A. V.; Efros, A. L. Effect of Dielectric Confinement on Optical Properties of Colloidal Nanostructures. *J. Exp. Theor. Phys.* **2016**, *122* (3), 554–566.
(35) Goubet, N.; Jagtap, A.; Livache, C.; Martinez, B.; Portalès, H.; Xu, X. Z.; Lobo, R. P. S. M.; Dubertret, B.; Lhuillier, E. Terahertz HgTe Nanocrystals: Beyond Confinement. *J. Am. Chem. Soc.* **2018**, *140* (15), 5033–5036.
(36) Goubet, N.; Jagtab, A.; Livache, C.; Martinez, B.; Portalès, H.; Xu, X. Z.; Dubertret, B.; Lhuillier, E. HgTe Nanocrystals: Beyond Confinement. **2018**, *submitted*.
(37) Kurilo, I. V.; Alekhin, V. P.; Rudyi, I. O.; Bulychev, S. I.; Osypyshin, L. I. Mechanical Properties of ZnTe, CdTe, CdHgTe and HgTe Crystals from Micromechanical Investigation. *Phys. Status Solidi A* **1997**, *163* (1), 47–58.
(38) *II-VI and I-VII Compounds; Semimagnetic Compounds - Supplement to | U. Rössler | Springer*.
(39) Wei, S.-H.; Zunger, A. Predicted Band-Gap Pressure Coefficients of All Diamond and Zinc-Blende Semiconductors: Chemical Trends. *Phys. Rev. B* **1999**, *60* (8), 5404–5411.
(40) Ko, J.-H.; Yoo, D.; Kim, Y.-H. Atomic Models for Anionic Ligand Passivation of Cation-Rich Surfaces of IV–VI, II–VI, and III–V Colloidal Quantum Dots. *Chem. Commun.* **2016**, *53* (2), 388–391.
(41) Liu, H.; Brozek, C. K.; Sun, S.; Lingerfelt, D. B.; Gamelin, D. R.; Li, X. A Hybrid Quantum-Classical Model of Electrostatics in Multiply Charged Quantum Dots. *J. Phys. Chem. C* **2017**, *121* (46), 26086–26095.
(42) Lhuillier, E.; Ithurria, S.; Descamps-Mandine, A.; Douillard, T.; Castaing, R.; Xu, X. Z.; Taberna, P.-L.; Simon, P.; Aubin, H.; Dubertret, B. Investigating the N- and P-Type Electrolytic Charging of Colloidal Nanoplatelets. *J. Phys. Chem. C* **2015**, *119* (38), 21795–21799.
(43) Konstantatos, G.; Sargent, E. H. PbS Colloidal Quantum Dot Photoconductive Photodetectors: Transport, Traps, and Gain. *Appl. Phys. Lett.* **2007**, *91* (17), 173505.
(44) Liu, H.; Lhuillier, E.; Guyot-Sionnest, P. 1/F Noise in Semiconductor and Metal Nanocrystal Solids. *J. Appl. Phys.* **2014**, *115* (15), 154309.

TOC graphic

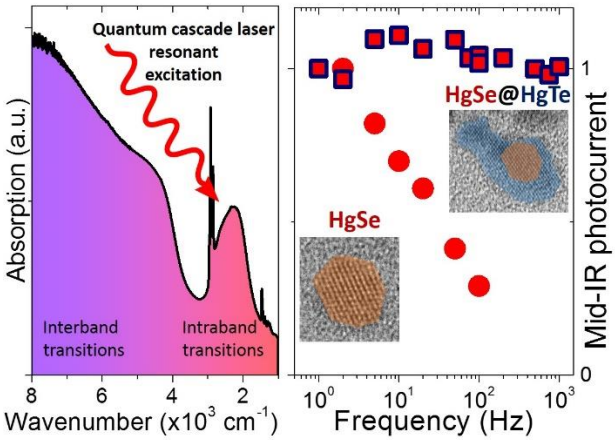
Quantum cascade laser
resonant
excitation
Absorption (a.u.)
Interband
transitions
Intraband
transitions
8
6
4
2
Wavenumber (x10^3 cm^{-1})
HgSe@HgTe
HgSe
1
0
Mid-IR photocurrent
10^0
10^1
10^2
10^3
Frequency (Hz)